ARTICLES
https://doi.org/10.1038/s41592-019-0421-z
nature methods

Bioluminescent-based imaging and quantification of glucose uptake in vivo

Tamara Maric[1,5], Georgy Mikhaylov[1,4,5], Pavlo Khodakivskyi[1], Arkadiy Bazhin[1], Riccardo Sinisi[1], Nicolas Bonhoure[2], Aleksey Yevtodiyenko[1], Anthony Jones[3], Vishaka Muhunthan[3], Gihad Abdelhady[3], David Shackelford[3] and Elena Goun[1*]

Glucose is a major source of energy for most living organisms, and its aberrant uptake is linked to many pathological conditions. However, our understanding of disease-associated glucose flux is limited owing to the lack of robust tools. To date, positron-emission tomography imaging remains the gold standard for measuring glucose uptake, and no optical tools exist for non-invasive longitudinal imaging of this important metabolite in in vivo settings. Here, we report the development of a bioluminescent glucose-uptake probe for real-time, non-invasive longitudinal imaging of glucose absorption both in vitro and in vivo. In addition, we demonstrate that the sensitivity of our method is comparable with that of commonly used ^{18}F-FDG-positron-emission-tomography tracers and validate the bioluminescent glucose-uptake probe as a tool for the identification of new glucose transport inhibitors. The new imaging reagent enables a wide range of applications in the fields of metabolism and drug development.

Glucose is the primary energy source for most organisms, and is used in both aerobic and anaerobic respiration. Impaired glucose consumption is one of the principal markers for various diseases, including cancer, diabetes and obesity[1–3]. Thus, the ability to non-invasively assess glucose use is of high interest. Several techniques have been developed to selectively image and quantify glucose uptake[4–7], with positron-emission tomography (PET) of ^{18}F-FDG radionuclide remaining the most common for measuring glucose uptake in clinical and preclinical settings[8]. However, it is not easily applicable in laboratory settings because of the short half-life of the reagent (110 min), the necessity of an on-site cyclotron, high cost and the exposure of personnel to ionizing radiation.

The major shortcomings of ^{18}F-FDG radionuclide imaging motivated the development of non-radioactive chemical tools for probing glucose uptake. These non-radioactive methods include hyperpolarized MRI (^{13}C-labeled D-glucose), stimulated Raman scattering, mass spectrometry and fluorescent optical imaging[4–7]. Optical imaging reagents remain among the most prominent because they complement microscopy-based cell imaging, are cost-effective, are convenient to use and offer a high-throughput alternative to all other modalities in a preclinical setting[5,9]. Reagents such as fluorescent 2-deoxy-glucose analogs, 2-NBDG[10] and 6-NBDG[11], were developed and used in various imaging studies to monitor glucose uptake via glucose transporter (GLUT), although they absorb and emit green light that is not optimal for detecting signals from living tissues. Therefore, their application in vivo is associated with weak fluorescence intensity, high background autofluorescence, low tissue penetration (<1 mm) and high dosage requirements[6]. To improve signal penetration in tissues, some recently reported studies have made use of near-infrared fluorescent (NIR) 2-deoxy-D-glucose conjugates (2-DG)[12–14]. However, because of the large size of NIR fluorophores (molecular mass 600–700 Da) in comparison to glucose (molecular mass 180.16 Da), these molecules do not mimic naturally occurring GLUT-mediated glucose flux[9,12].

To develop sensitive, non-radioactive and easy-to-use optical tools to image glucose uptake non-invasively in vitro and in vivo, we chose bioluminescent imaging (BLI), in which luciferase enzyme reporters oxidize small-molecule substrates (luciferins) in a process that produces light[15]. BLI has high sensitivity, an outstanding signal/noise ratio and favorable properties for non-invasive in vivo imaging[15–17]. While multiple luciferase-expressing animal models of human diseases have been recently reported and even made commercially available[15,16], the applications of BLI techniques for the in vivo imaging of metabolic uptake remain limited[4,15,18].

In this study, we present a BLI-based optical imaging reagent for the non-invasive imaging and quantification of glucose uptake, named the 'bioluminescent glucose-uptake probe' (BiGluc). Our findings demonstrate that BiGluc can accurately measure glucose uptake in living cells and that this technology is more sensitive than other commonly used fluorescence-based techniques in vitro. In addition, BiGluc can successfully image and quantify metabolic fluxes of glucose in living mice in a non-invasive and longitudinal fashion, and a detectable signal is observed even in the deep organs of living animals, such as the gastrointestinal tract. The BiGluc tool can also be used to reliably measure glucose uptake in animal models of diseases such as cancer, and can be used as a tool for the screening of GLUT inhibitors, which is a fast-growing field in cancer drug discovery. Finally, we demonstrate that the sensitivity of our BLI-based method is comparable to that of the commonly used ^{18}F-FDG-PET tracer, making this new technology the first successful example, to our knowledge, of an optical tool for in vivo glucose uptake. Our approach substantially broadens the current applications of BLI, extending its potential for imaging glucose and

[1]Institute of Chemical Sciences and Engineering (ISIC), Swiss Federal Institute of Technology (EPFL), Lausanne, Switzerland. [2]Nestlé Institute of Health Sciences SA, EPFL Innovation Park, Bâtiments G/H, Lausanne, Switzerland. [3]Department of Pulmonary and Critical Care Medicine, David Geffen School of Medicine, University of California, Los Angeles, CA, USA. [4]Present address: Jožef Stefan Institute, Ljubljana, Slovenia. [5]These authors contributed equally: Tamara Maric, Georgy Mikhaylov. *e-mail: elena.goun@epfl.ch

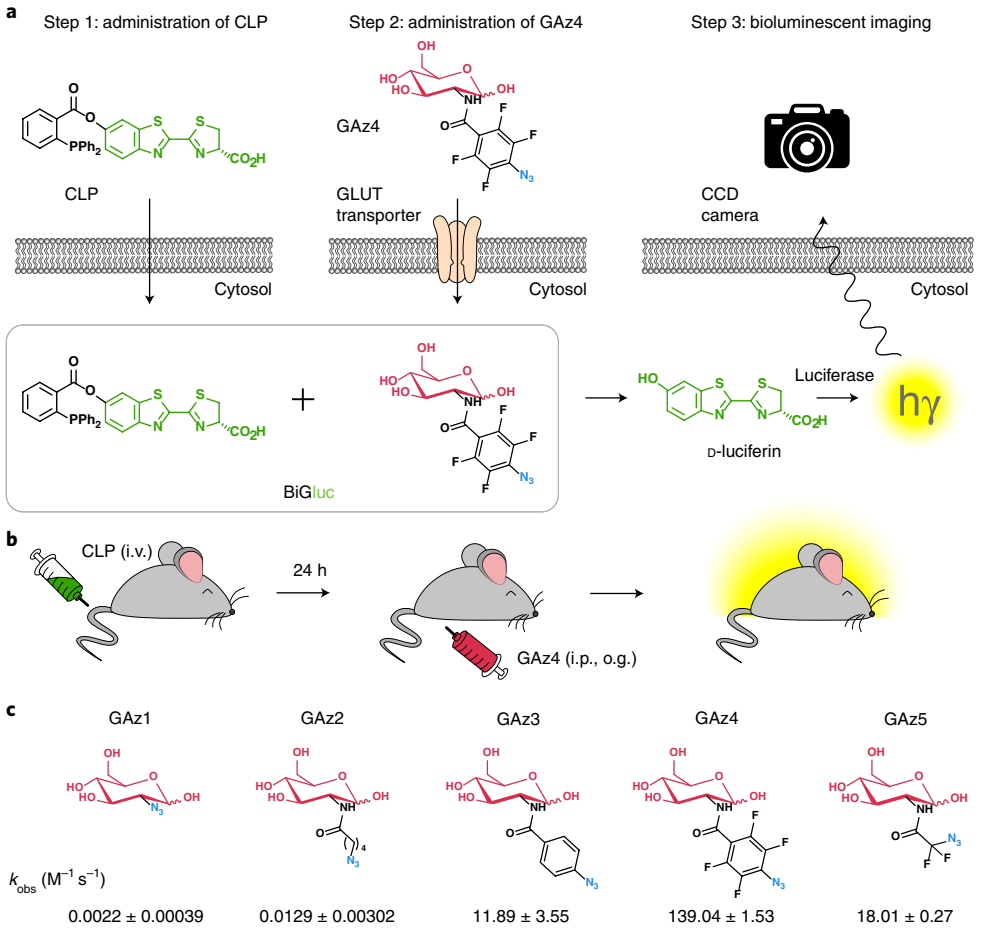

Fig. 1 | Design strategy for D-glucose BiGluc. a, Schematic representation of the in vitro application of BiGluc technology. The technology is based on the bioorthogonal reaction (Staudinger ligation). Two reagents, CLP and GAz4, undergo a reaction inside the cell resulting in the release of free luciferin, which is subsequently processed by luciferase to produce light. **b**, The BiGluc method is suitable for in vivo application. Animals expressing luciferase are first injected with CLP and after 24 h they are administered with GAz4. Immediately after GAz4 administration, animals are monitored using camera imaging system to quantify light produced on reaction of BiGluc components inside cells. o.g., oral gavage; i.p., intraperitoneal. **c**, Structures of the synthesized azido-glucoses (GAz1–GAz5) investigated for the best reactivity with CLP reagent in the Staudinger ligation reaction. Reaction rate constants are presented as mean ± s.e.m. ($n = 3$, independent experiments).

many other small-molecule metabolites that play important roles in human pathologies.

Results

Design and synthesis of the BiGluc. The recent development of BLI probes to sense molecular signatures of target tissues relies on the simple principle that luciferin 'caged' on the phenolic oxygen is not a substrate for luciferase until it is uncaged by a specific biological process of interest[15,18]. The design strategy for D-glucose-mediated bioluminescent signal production is based on a bio-orthogonal click reaction (Staudinger ligation)[19] between a properly tuned activatable caged luciferin triarylphosphine ester and an azido-modified glucose molecule that results in the release of free luciferin, triggering the production of quantifiable bioluminescence signal in the presence of firefly luciferase (Fig. 1 and Supplementary Video 1). When glucose uptake was evaluated in vitro, the cells were first incubated with caged luciferin triphenylphosphine (CLP), which is internalized via passive diffusion (Supplementary Fig. 1), washed and subsequently incubated with the glucose azide 4 (GAz4) reagent (Fig. 1a). To measure glucose uptake in vivo, we injected the animals with the CLP reagent (intravenously (i.v.)) 24 h before the administration of GAz4 via intraperitoneal (i.p.) injection or oral gavage (o.g.) followed by real-time signal acquisition (Fig. 1b). The light production was proportional to the amount of GAz4 reagent taken up inside the cells or tissue and directly reflected the activity of GLUT transporters.

To identify a GAz compound that would possess robust reactivity with the CLP probe and also preserve the specificity to the native GLUTs, we synthesized a series of reagents with an azide substitution of the 2-hydroxy group—a substitution that had been successfully used in the design of the ^{18}F-FDG and 2-NBDG glucose probes[20] (Fig. 1c). Synthetic procedures and chemical characterizations of new GAz glucose analogs are described in detail in Supplementary Notes 1 and 2. All of the GAz derivatives differ in steric hindrance and electron deficiency of the azide. While a kinetic analysis of the reaction between CLP and GAz1 or GAz2 demonstrated low reaction rates, GAz3, GAz5 and GAz4 enhanced the reaction rate by three and five orders of magnitude ($\times 10^5$), respectively (Fig. 1c). Therefore, GAz4 was used for further in vitro and in vivo validation studies.

Imaging and quantification of D-glucose uptake in living cells using the BiGluc probe. To test whether the new probe could produce light in live cells, we measured the amount of BiGluc light production from three different cell lines stably transfected with luciferase (4T1-luc, HT1080-luc and C2C12-luc) under different conditions. First, we determined that incubation of cells with

10 µM CLP for 1 h followed by a wash and subsequent treatment with 100 µM GAz4 reagent resulted in the highest signal/background noise ratio (Supplementary Fig. 2). Second, we found that both GAz4 reagent and CLP were not toxic to cells and did not perturb cellular proliferation in the concentration range used in the assay (Supplementary Fig. 3). Third, GAz4 did not alter cellular redox potential and had no effect on the total NAD^+ concentration (Supplementary Fig. 4). Last, we investigated the cross-reactivity of GAz4 with naturally occurring thiols such as free cysteine and glutathione, and observed no detectable reduction products for the duration of the test (up to 60 min; Supplementary Fig. 5).

We then investigated whether the resulting light output from the BiGluc probe in living cells was D-glucose specific by using a series of competition experiments that have been previously used for testing the behavior of reported glucose probes[6,10,14]. Real-time light production from the BiGluc probe was measured in competition with both D-glucose and the non-natural stereoisomer L-glucose as a negative control in the same cell lines as before (4T1-luc, HT1080-luc and C2C12-luc). Figure 2a shows that the total light output from the BiGluc probe decreased significantly as the concentration of D-glucose in the buffer increased. At the same time, the signal was not affected by the increasing concentration of L-glucose (Fig. 2b). These results were consistent in all three cell types, demonstrating a direct correlation between D-glucose uptake and light production from the BiGluc probe in vitro.

In the next step, we investigated the specificity of the D-glucose signal by directly inhibiting GLUT transporters with cytochalasin B, a potent endofacial inhibitor of the glucose transporter family[21]. First, we used a radioisotope-based assay to validate that the treatment of 4T1-luc cells with cytochalasin B indeed induced GLUT inhibition. As expected, incubation of 4T1-luc cells with 10 µM cytochalasin B for 10 min resulted in a 23% decrease in radioactive signal (Supplementary Fig. 6a). We then repeated the same cytochalasin B inhibition experiment using the BiGluc probe in two different cell lines (4T1-luc and HT1080-luc) and quantified the bioluminescent signal. The results obtained were in agreement with the radioactive assay and demonstrated 18% and 40% signal reduction for 4T1-luc and HT1080-luc, respectively (Supplementary Fig. 6b), further suggesting a direct correlation between bioluminescent light output from the BiGluc probe and D-glucose uptake. Next, we compared the performance of BiGluc with a commercially available GB2-Cy3 probe[22]. Treatment of 4T1-luc cells with exofacial inhibitor of GLUT transporter 4,6-O-ethylidene-α-D-glucose (4,6-EDG) resulted in a decrease of the signal from GB2-Cy3 probe (9%; Supplementary Fig. 6c). We also observed a somewhat larger bioluminescent signal decrease with BiGluc probe (25%; Supplementary Fig. 6d).

We further explored whether a specific knockout of the GLUT1 transporter, known to be overexpressed in many types of cancer[23], would influence signal production from the BiGluc probe. We performed CRISPR/Cas9-mediated *Slc2a1* gene knockout in 4T1-luc cells to produce a GLUT1-deficient version of this cell line (referred to as GLUT1$^{-/-}$). The knockout was validated by western blotting and sequencing that confirmed the introduction of mostly frameshift indels, resulting in a functional 'knockout' of the gene (Supplementary Fig. 7). Incubation of the 4T1-luc-GLUT1$^{-/-}$ no. 1 cells with the BiGluc probe demonstrated a significantly reduced light output (40%) compared with that of the control (Fig. 2c and Supplementary Fig. 8a). Next, glucose-uptake studies in parental cells, negative control and knockout clones confirmed the results of clone validation (Supplementary Fig. 8b). To further confirm the direct correlation between the BiGluc signal and the activity of GLUT transporters, we performed short hairpin RNA (shRNA)-mediated *Slc2a1* knockdown in 4T1-luc cells. As expected, it resulted in a 40–50% reduction in glucose uptake as measured by the BiGluc probe (Supplementary Fig. 8c,d). The magnitude of signal reduction was consistent with previously reported data[24–26].

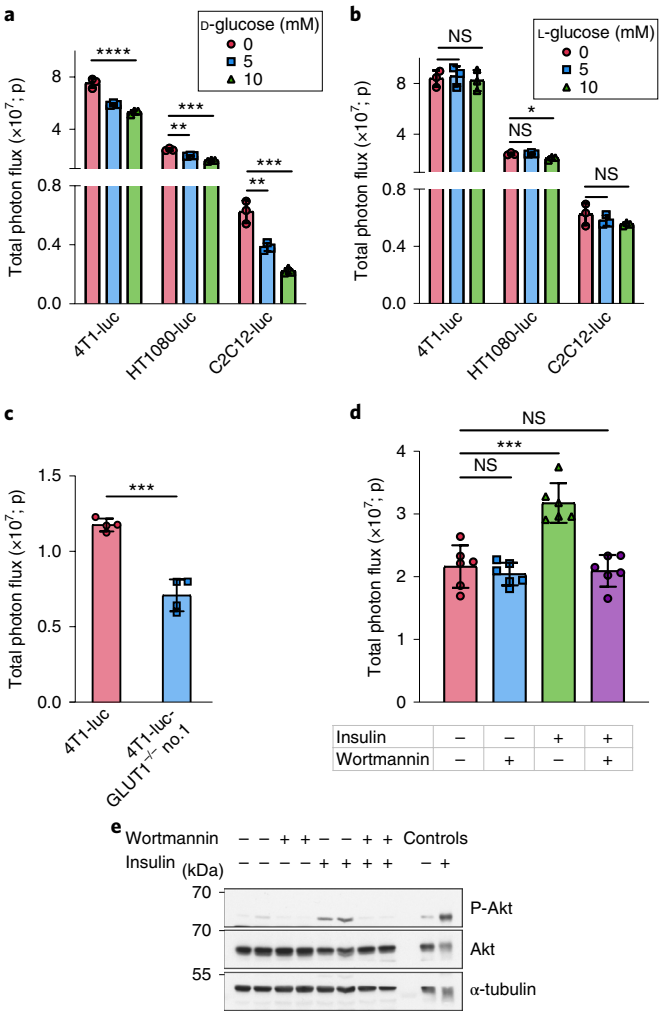

Fig. 2 | Imaging and quantification of D-glucose uptake in living cells using the BiGluc probe. a, Total photon flux (photons, p) obtained from BiGluc probe in three different cell lines stably transfected with luciferase construct (4T1-luc, HT1080-luc and C2C12-luc). The cells were first incubated for 1 h with CLP, washed with PBS and then treated with GAz4 in the presence or absence of the natural competitor D-glucose (0, 5 and 10 mM) followed by signal acquisition. Bars represent the area under the curve (total photon flux) over 20 min ($n = 3$). **b**, The same as **a**, but D-glucose was replaced with L-glucose in identical concentrations (0, 5 and 10 mM) ($n = 3$). **c**, Comparison of light production using BiGluc probe in 4T1-luc and GLUT1-knockout 4T1-luc cells (4T1-luc and 4T1-luc-GLUT1$^{-/-}$ no. 1, respectively; $n = 4$). The experiment was performed as described in **a**. **d**, Total photon flux from C2C12-luc myotubes treated with 10 µM wortmannin for 30 min and 100 nM insulin for 30 min as outlined in the table, followed by the addition of BiGluc probe as described in **a** and signal acquisition ($n = 6$). **e**, Western blot analysis of the phosphorylation status of Akt in C2C12-luc cells. The total photon flux from cells was normalized to the appropriate luciferin control in cases where the experimental conditions influenced the signal of luciferin production. Data in **a**–**d** are presented as mean ± s.d.; *n* values represent the number of biologically independent samples. Experiments in **a**–**e** were performed independently at least twice. $^*P < 0.05$, $^{**}P < 0.01$, $^{***}P < 0.001$, $^{****}P < 0.0001$. NS, non-significant by two-tailed *t*-test. For uncut blot images, see Supplementary Fig. 15. For individual *P* values, see the Source Data for this figure.

As skeletal muscles and adipocytes are known to exhibit insulin-dependent regulation of GLUT4 translocation to the plasma membrane[27], we analyzed the effect of PI3K-dependent insu-

lin stimulation on light production using the BiGluc probe. We investigated the performance of the probe in differentiated C2C12 myotubes that were stably overexpressing luciferase (C2C12-luc). C2C12-luc differentiation was confirmed by western blot analysis (Supplementary Fig. 9). As expected, a 32% increase in signal was observed in insulin-treated C2C12-luc cells as compared with that of the non-insulin-treated control (Fig. 2d). In the presence of wortmannin, an inhibitor of PI3K[28], the signal elevation was completely suppressed (Fig. 2d). To confirm wortmannin-induced PI3K inhibition, we performed an immunoblot analysis of treated C2C12-luc cells, using antibodies directed against AKT, a known PI3K downstream target. AKT phosphorylation levels are insulin dependent and were abolished on wortmannin treatment (Fig. 2e). In addition, we tested the performance of the BiGluc probe by using adipocytes differentiated from 3T3-L1-luc fibroblasts. We observed a three fold increase in signal intensity on insulin stimulation (Supplementary Fig. 10), which was fully consistent with previous reports[29–31]. These results further demonstrate the D-glucose uptake specificity of the BiGluc signal.

To further investigate whether the new BLI-based probe could provide reliable information on D-glucose uptake in vitro, we compared the light output resulting from the BiGluc probe with that of the radioisotope (tritium-labeled glucose, [^{3}H]-2DG) and fluorescence-based (2-NBDG) probes under the same experimental conditions. In this experiment, C2C12-luc cells were treated with various concentrations of insulin (0–200 nM) followed by incubation with three different reagents (BiGluc, [^{3}H]-2DG and 2-NBDG) and signal acquisition. The results exhibited a linear increase in signal with increasing concentrations of insulin for both BiGluc and [^{3}H]-2DG that was expected owing to the insulin-dependent GLUT4 translocation to the plasma membrane[27]. While the radioisotope-based method demonstrated higher sensitivity, the BiGluc approach was equally reliable because the z' factors (a well-known indicator of assay reliability[32]) for both assays were higher than 0.5 (Supplementary Fig. 11). On the other hand, the fluorescence-based approach using 2-NBDG failed to produce an insulin-dependent increase in signal under these experimental conditions. These data are in agreement with previously published work that reported poor sensitivity with 2-NBDG readouts in comparison to that of [^{3}H]-2DG for measuring glucose uptake[6,33]. Taken together, the results demonstrate that the light production from the BiGluc probe is specific to the GLUT transporter activity and can be used as a reliable, non-invasive and non-radioactive method to measure D-glucose uptake in live cells.

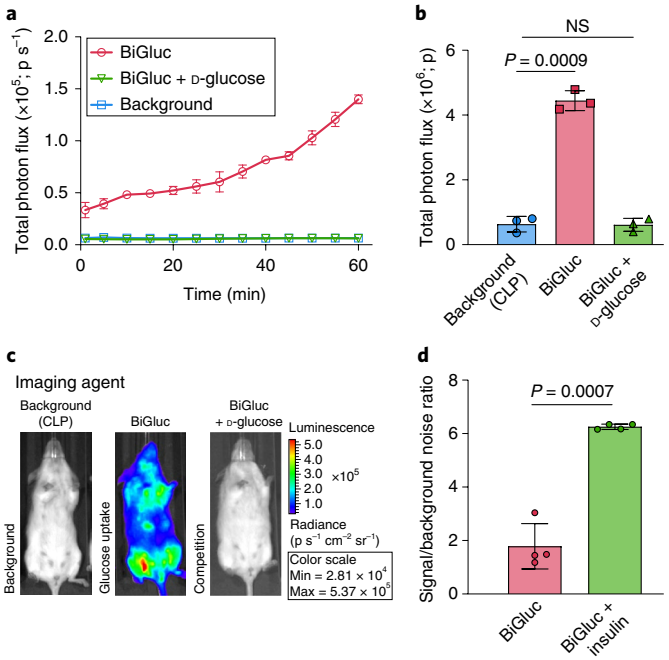

Fig. 3 | Imaging and quantification of D-glucose uptake in transgenic reporter mice (FVB-luc$^{+/+}$) using the BiGluc probe. a, Non-invasive quantification of the whole-body bioluminescent signal (photons per second (p s^{-1})) over time in three different groups of FVB-luc$^{+/+}$ mice (background, BiGluc and BiGluc plus D-glucose). Mice were first injected i.v. with CLP solution, and 24 h later mice received an oral gavage of GAz4 (BiGluc group), GAz4 + D-glucose (BiGluc + D-glucose group) or PBS (background group). Bioluminescent signal acquisition started immediately after the oral gavage to mice ($n = 3$). **b**, Integration of the kinetic curves (area under the curve) shown in **a** over 60 min ($n = 3$). Signal/background noise ratio was 7.5-fold. **c**, Representative images from the three groups of mice. **d**, Effect of insulin treatment on glucose uptake measured with BiGluc. FVB-luc$^{+/+}$ mice were injected i.v. with CLP. After 24 h they were injected i.p. with either GAz4 or GAz4 plus insulin, and then they underwent 1 h of imaging. Signal/background noise ratio was calculated for each group. Data are presented as mean ± s.d. ($n = 4$ per group). Each n represents a biologically independent sample. Experiments in **a**–**d** were performed independently at least twice.

Imaging and quantification of D-glucose uptake in transgenic reporter mice (FVB-luc$^{+/+}$). To establish the efficacy of the BiGluc probe for in vivo applications, we used a genetically engineered mouse model that ubiquitously expresses luciferase through the β-actin promoter (FVB-luc$^{+/+}$ mice)[34]. To investigate the clearance of CLP probe from the blood to avoid non-specific extra cellular reaction between CLP and GAz4, we measured bioluminescent signal from the mice i.v.-injected with CLP compound. We observed a significant (4×10^3–fold) drop in signal by 24 h after the injection of CLP, which was consistent with significant decrease of CLP plasma concentration (Supplementary Fig. 12a,b). These results suggest that 24 h is enough for the CLP reagent to clear from the blood and accumulate inside the cells. We found that i.p. injection of GAz4 24 h after i.v. administration of CLP resulted in a stable increase in signal for up to 1 h followed by a 2-h plateau (Supplementary Fig. 12c). These results were consistent with signal measured from different organs at 15 and 45 min after the injection of GAz4 (Supplementary Fig. 12d).

In the next step, we investigated whether the optical signal produced in vivo by the BiGluc probe was D-glucose specific by administering the probe in the presence or absence of high concentrations of D-glucose (competition experiment). The results shown in Fig. 3a–c indicate that the competition with D-glucose (1:300 ratio with the GAz4 probe) resulted in suppression of the BiGluc signal to the background level (CLP alone), thus demonstrating the successful competition of BiGluc probe with a natural substrate.

To further investigate the D-glucose selectivity of the BiGluc probe in vivo, we performed an insulin tolerance test. High levels of insulin should result in GLUT4 translocation to the cellular membrane and a subsequent increase in D-glucose uptake by the tissues[35]. FVB-luc$^{+/+}$ mice received an i.v. injection of CLP followed by an i.p. injection of the GAz4 reagent 24 h later, either in pure PBS (control) or in combination with insulin, followed by signal acquisition. We observed a three fold increase in signal for the mice pretreated with insulin compared to the control group (Fig. 3d). Together, these results demonstrate that the BiGluc probe can be used to reliably quantify physiological fluxes of D-glucose in live animals in a non-invasive fashion.

Imaging and quantification of D-glucose uptake in tumor xenograft models using the BiGluc probe. Glucose transporters, especially GLUT1, play a critical role in the development of several types

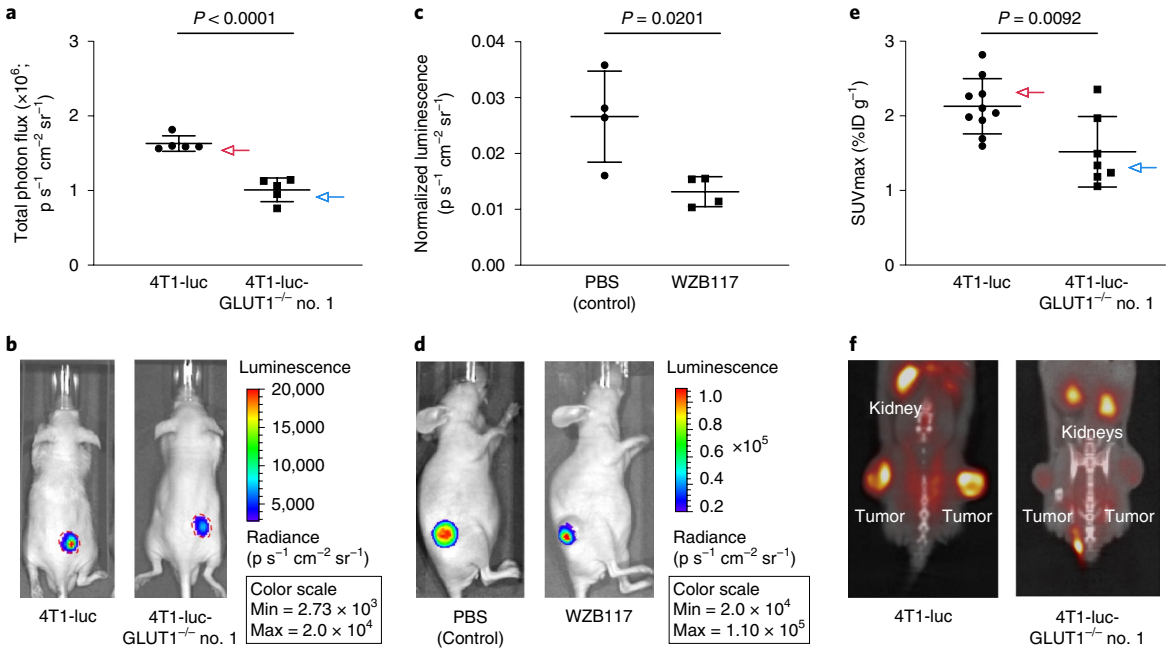

Fig. 4 | Imaging and quantification of D-glucose uptake in tumor xenograft models using the BiGluc and ^{18}F-FDG probes. a, Comparison of glucose uptake by subcutaneous tumors formed by 4T1-luc and 4T1-luc-GLUT1$^{-/-}$ no. 1 cells. The cells were injected into Swiss nu/nu mice subcutaneously and allowed to grow. When tumors reached 65 mm^3 in size, mice received i.p. injections of GAz4 24 h after i.v. injections of CLP. A decrease in signal of 38% was observed in the 4T1-luc GLUT1-deficient tumors compared to 4T1-luc controls. Graph represents total photon flux over 10 min from xenografts ($n = 5$). **b**, Representative images of mice bearing 4T1-luc or 4T1-luc-GLUT1$^{-/-}$ no. 1 tumors are shown. The red line represents the margin of the tumors, indicating similar tumor size in both groups. **c**, Investigation of BiGluc light output on treatment with GLUT1 transporter specific inhibitor (WZB-117). Swiss nu/nu mice were injected with 4T1-luc cells. When tumors reached a size of 65 mm^3, the mice were divided into two groups (four animals in each) and were i.v.-injected with CLP. Then 24 h later they received i.p. injection of GAz4 or a combination of GAz4 and WZB-117. Graph represents areas under the kinetic curves over 60 min normalized to photon flux resulting from injection of an equimolar amount of luciferin ($n = 4$). **d**, Representative images of mice with and without inhibitor WZB-117 treatment. **e**, Glucose uptake by 4T1-luc and 4T1-luc-GLUT1$^{-/-}$ no. 1 tumors measured by PET. We calculated maximum standard uptake values (SUVmax) by measuring %ID g^{-1} of ^{18}F-FDG in tumors ($n = 10$ 4T1-luc tumors and $n = 7$ 4T1-luc-GLUT1$^{-/-}$ no. 1 tumors). **f**, Representative images of ^{18}F-FDG PET/CT scans of mice bearing 4T1-luc or 4T1-luc-GLUT1$^{-/-}$ no. 1 tumors. Data are presented as mean ± s.d. *P* values were calculated using a two-tailed *t*-test. Each *n* represents a biologically independent sample. All experiments were repeated independently at least twice.

of cancer[36]. Therefore, new reagents that would allow the non-invasive imaging and quantification of GLUT activity in live animals are of high value. To investigate the performance of the BiGluc probe in tumors, we inoculated Swiss nu/nu mice with either 4T1-luc or 4T1-luc-GLUT1$^{-/-}$ no. 1 (the same cells previously used for in vitro experiments; see Fig. 2c). The tumors were grown to an average volume of 65 mm^3. All the animals were initially injected with an equimolar dose of luciferin to ensure that the tumor size and level of luciferase expression were equal between the groups. Like the previous in vivo experiments, the mice received an i.v. injection of the CLP probe followed by an i.p. injection with the GAz4 reagent 24 h later. The animals were anesthetized, and the light output was quantified continuously for 1 h. Noticeably, the signal from the mice implanted with 4T1-luc-GLUT1$^{-/-}$ no. 1 tumors demonstrated a 38% decrease in the total photon flux compared with that in the control group (Fig. 4a,b), which was consistent with the previous in vitro assay results (Fig. 2c). A postmortem analysis of the excised tumors by western blotting and immunohistochemistry confirmed the effective deletion of GLUT1 in 4T1-luc-GLUT1$^{-/-}$ no. 1 tumors (Supplementary Fig. 13a,b).

We also investigated whether the BiGluc signal could be directly modulated through the chemical inhibition of GLUT1 transporters in vivo. WZB-117 is a small-molecule reversible inhibitor of GLUT1 that is known to efficiently block glucose transport in diverse cancer models[37]. Nude mice were inoculated with 4T1-luc cells, and tumors were allowed to grow to a volume of about 65 mm^3. The mice from two groups ($n = 4$) received i.v. injections of CLP followed by an i.p. injection of GAz4 24 h later in either PBS alone (control group) or WZB-117 in PBS (WZB-117 group). We observed a 50% reduction in signal from the group of tumor xenografts from mice treated with the GLUT1 inhibitor (Fig. 4c,d). No difference in signal production was observed from the control group of mice administered luciferin alone in the presence or absence of WZB-117 (Supplementary Fig. 13c). These results further confirm the selectivity of BiGluc signal production from D-glucose uptake in animal models of cancer.

Direct comparison of BiGluc and ^{18}F-FDG-PET in tumor xenograft models. To investigate the performance of the BiGluc probe in comparison to the commonly used clinical techniques, we performed ^{18}F-FDG PET/CT imaging on live mice transplanted with either 4T1-luc cells or 4T1-luc-GLUT1$^{-/-}$ no. 1 cells ($n = 10$). We observed that the 4T1-luc-GLUT1$^{-/-}$ no. 1 tumors exhibited a significantly lower overall uptake of ^{18}F-FDG compared to the 4T1-luc tumors (Fig. 4e,f). This observation was further confirmed by the quantification of the maximum standard uptake value (SUVmax) (Fig. 4e). Like in previous experiments, the tumor sizes were equally matched between mice with 4T1-luc and 4T1-luc-GLUT1$^{-/-}$ no. 1 tumors, demonstrating that the reduction in ^{18}F-FDG uptake in 4T1-luc-GLUT1$^{-/-}$ no. 1 tumors was not the result of a reduced tumor volume (Supplementary Fig. 13d).

In previously reported studies, GLUT1 transporter expression directly correlated with ^{18}F-FDG uptake in tumors in vivo[25]. To confirm the deletion of the GLUT1 transporter, we performed immunohistochemistry (IHC) staining to measure the GLUT1 expression

levels on both 4T1-luc and 4T1-luc-GLUT1$^{-/-}$ no. 1 tumors. We found significantly lower GLUT1 protein levels in the 4T1-luc-GLUT1$^{-/-}$ no. 1 tumors compared to their controls (Supplementary Fig. 14a). We identified two mice in the 4T1-luc-GLUT1$^{-/-}$ no. 1 group that had elevated ^{18}F-FDG uptake (Supplementary Fig. 14b). IHC staining of these tumors showed increased GLUT1 protein expression levels (Supplementary Fig. 14c). We think that the probable explanation for why two of the tested 4T1-GLUT1$^{-/-}$ tumors displayed elevated GLUT1 levels is the selection pressure on the tumor, which could revert a single mutation in one allele[38]. Overall, these results demonstrate that the BiGluc technique performs very similarly to the gold-standard technique in the field of in vivo glucose uptake imaging, such as ^{18}F-FDG/PET.

Discussion

Easily accessible non-invasive in vivo imaging techniques for studies of glucose uptake are limited[4]. Here, we describe a new tool to visualize glucose uptake based on non-invasive bioluminescent imaging, which is a very sensitive and quantitative modality[15–17]. The overall approach is based on the combination of caged luciferin technology and the bio-orthogonal 'click' reaction between an organic azide and appropriately tuned triarylphosphine esters (Staudinger ligation)[19]. Although the Staudinger ligation is one of the most efficient reactions in living animals[39], it has a slow kinetics that significantly limits its application for in vivo imaging[40]. We introduced a perfluorophenyl azide moiety in the structure of corresponding azido-glucose derivative (GAz4) to increase reactivity of the azido-modified glucose reagent. This chemical tuning allowed the GAz4 probe to produce a robust bioluminescent signal on reaction with the CLP both in vitro and in vivo.

To demonstrate the selectivity of the BiGluc probe toward glucose uptake in living cells, we performed a series of cell-based assays, such as a competition between D- and L-glucose, selective CRISPR/Cas9-mediated and shRNA-mediated *Slc2a1* gene knockouts, treatments of cells with different exofacial and endofacial GLUT inhibitors, and studies of PI3K-dependent insulin-induced and wortmannin-inhibited glucose uptake. All these results demonstrate that the BiGluc probe can accurately and selectively measure glucose uptake and be used to measure important physiologically relevant processes in live cells.

To directly compare our BiGluc approach with other commonly used methods to measure glucose uptake in living cells, we performed side-by-side experiments where insulin-treated C2C12-luc myotubes were incubated with three different reagents (BiGluc, ^{3}H-2DG and 2-NBDG). Our results indicate that the BiGluc method is equally reliable compared to the [^{3}H]-2DG approach and superior to that of 2-NBDG. The BiGluc probe was shown to be more sensitive than the previously reported GB2-Cy3 reagent, which could be explained by significantly smaller modifications of the D-glucose structure of GAz4 in comparison to the rather bulky GB2-Cy3 dye[22].

Inspired by these exciting in vitro results, we tested the application of the BiGluc probe for the non-invasive imaging of glucose uptake in vivo. The selectivity of the BiGluc probe toward glucose uptake was confirmed by competition experiments with high concentrations of D-glucose and insulin stimulation experiments in transgenic reporter mice (FVB-luc$^{+/+}$). To demonstrate the application of the BiGluc technology in cancer models, we evaluated the performance of the probe in mice bearing xenograft tumors of 4T1-luc and 4T1-luc GLUT1 knockouts (4T1-luc GLUT1$^{-/-}$ no. 1). There are several reports in the literature that describe successful tumor formation of GLUT1 knockout tumor[41,42]. As expected, we observed significant decrease in signal production from BiGluc in GLUT1 knockout mice in comparison to 4T1-luc controls. In addition, we validated the application of the BiGluc tool for the identification of new GLUT inhibitors in vivo. In this experiment, mice bearing 4T1-luc breast cancer xenografts were injected with a small-molecule inhibitor of GLUT1 that is known to efficiently block glucose transport in diverse cancer models (WZB-117)[37]. The light output resulting from the BiGluc probe in WZB-117-treated mice was significantly lower than in the vehicle-treated controls, further suggesting direct correlation between light production and activity of GLUT transporters. Finally, direct comparison of the performance of the BiGluc probe with ^{18}F-FDG-PET in the same animal model established an identical performance between both reagents. Taken together, the data revealed robust non-invasive detection of physiologically relevant changes of glucose uptake in the animal model of cancer. To the best of our knowledge, this is the first example of an optical imaging reagent that is suitable for non-invasive longitudinal imaging of glucose uptake both in vitro and in vivo.

Our findings demonstrate the use of the BiGluc probe as a powerful tool for studies of glucose uptake in living organisms. Since glucose plays a key role in many human pathological conditions, we believe that this technology can be widely used for drug discovery and for monitoring the development and progression of diseases linked to aberrant glucose uptake such as cancer, diabetes and obesity[1–3]. In addition, the BiGluc technology expands the niche of biomolecules that can be probed by bioluminescent imaging, which is a fast-growing field of research. In the future, the BiGluc probe sensitivity could be further increased by using novel red-shifted luciferin–luciferase combinations[15,43]. Since other small-molecule metabolites can be chemically labeled with azido precursors, this technology represents a powerful new platform for the non-invasive longitudinal imaging of metabolite fluxes.

Online content

Any methods, additional references, Nature Research reporting summaries, source data, statements of code and data availability and associated accession codes are available at https://doi.org/10.1038/s41592-019-0421-z.

Received: 1 September 2018; Accepted: 4 April 2019;
Published online: 13 May 2019

References

1. Hay, N. Reprogramming glucose metabolism in cancer: can it be exploited for cancer therapy? *Nat. Rev. Cancer* **16**, 635–649 (2016).
2. Kaur, J. A comprehensive review on metabolic syndrome. *Cardiol. Res. Pract.* **2014**, 21 (2014).
3. Chang, C.-H. & Pearce, E. L. Emerging concepts of T cell metabolism as a target of immunotherapy. *Nat. Immunol.* **17**, 364–368 (2016).
4. Momcilovic, M. & Shackelford, D. B. Imaging cancer metabolism. *Biomol. Ther.* **26**, 81–92 (2018).
5. Cox, B. L., Mackie, T. R. & Eliceiri, K. W. The sweet spot: FDG and other 2-carbon glucose analogs for multi-modal metabolic imaging of tumor metabolism. *Am. J. Nucl. Med. Mol. Imaging* **5**, 1–13 (2015).
6. Hu, F. et al. Vibrational imaging of glucose uptake activity in live cells and tissues by stimulated raman scattering. *Angew. Chem.* **54**, 9821–9825 (2015).
7. Kim, W. H., Lee, J., Jung, D. W. & Williams, D. R. Visualizing sweetness: increasingly diverse applications for fluorescent-tagged glucose bioprobes and their recent structural modifications. *Sensors* **12**, 5005–5027 (2012).
8. Vallabhajosula, S., Solnes, L. & Vallabhajosula, B. A broad overview of positron emission tomography radiopharmaceuticals and clinical applications: what is new? *Semin. Nucl. Med.* **41**, 246–264 (2011).
9. Tseng, J. C., Wang, Y., Banerjee, P. & Kung, A. L. Incongruity of imaging using fluorescent 2-DG conjugates compared to ^{18}F-FDG in preclinical cancer models. *Mol. Imaging Biol.* **14**, 553–560 (2012).
10. O'Neil, R. G., Wu, L. & Mullani, N. Uptake of a fluorescent deoxyglucose analog (2-NBDG) in tumor cells. *Mol. Imaging Biol.* **7**, 388–392 (2005).
11. Speizer, L., Haugland, R. & Kutchai, H. Asymmetric transport of a fluorescent glucose analogue by human erythrocytes. *Biochim. Biophys. Acta* **815**, 75–84 (1985).
12. Cheng, Z. et al. Near-infrared fluorescent deoxyglucose analogue for tumor optical imaging in cell culture and living mice. *Bioconjug. Chem.* **17**, 662–669 (2006).
13. Kovar, J. L., Volcheck, W., Sevick-Muraca, E., Simpson, M. A. & Olive, D. M. Characterization and performance of a near-infrared 2-deoxyglucose optical imaging agent for mouse cancer models. *Anal. Biochem.* **384**, 254–262 (2009).

14. Park, J., Lee, H. Y., Cho, M. H. & Park, S. B. Development of a cy3-labeled glucose bioprobe and its application in bioimaging and screening for anticancer agents. *Angew. Chem.* **46**, 2018–2022 (2007).
15. Mezzanotte, L., van 't Root, M., Karatas, H., Goun, E. A. & Lowik, C. In vivo molecular bioluminescence imaging: new tools and applications. *Trends Biotechnol.* **35**, 640–652 (2017).
16. Dothager, R. S. et al. Advances in bioluminescence imaging of live animal models. *Curr. Opin. Biotechnol.* **20**, 45–53 (2009).
17. Genevois, C., Loiseau, H. & Couillaud, F. In vivo follow-up of brain tumor growth via bioluminescence imaging and fluorescence tomography. *Int. J. Mol. Sci.* **17**, 1815 (2016).
18. Li, J., Chen, L., Du, L. & Li, M. Cage the firefly luciferin!—a strategy for developing bioluminescent probes. *Chem. Soc. Rev.* **42**, 662–676 (2013).
19. Saxon, E. & Bertozzi, C. R. Cell surface engineering by a modified Staudinger reaction. *Science* **287**, 2007–2010 (2000).
20. Sundhoro, M., Jeon, S., Park, J., Ramstrom, O. & Yan, M. Perfluoroaryl azide Staudinger reaction: a fast and bioorthogonal reaction. *Angew. Chem.* **56**, 12117–12121 (2017).
21. Estensen, R. D. & Plagemann, P. G. W. Cytochalasin B: inhibition of glucose and glucosamine transport. *Proc. Natl. Acad. Sci. USA* **69**, 1430–1434 (1972).
22. Park, J. et al. Impact of molecular charge on GLUT-specific cellular uptake of glucose bioprobes and in vivo application of the glucose bioprobe, GB2-Cy3. *Chem. Commun.* **50**, 9251–9254 (2014).
23. Yun, J. et al. Glucose deprivation contributes to the development of KRAS pathway mutations in tumor cells. *Science* **325**, 1555–1559 (2009).
24. Liu, Y. et al. A small-molecule inhibitor of glucose transporter 1 downregulates glycolysis, induces cell-cycle arrest, and inhibits cancer cell growth in vitro and in vivo. *Mol. Cancer Ther.* **11**, 1672–1682 (2012).
25. Goodwin, J. et al. The distinct metabolic phenotype of lung squamous cell carcinoma defines selective vulnerability to glycolytic inhibition. *Nat. Commun.* **8**, 15503 (2017).
26. Suzuki, S. et al. Involvement of GLUT1-mediated glucose transport and metabolism in gefitinib resistance of non-small-cell lung cancer cells. *Oncotarget* **9**, 32667–32679 (2018).
27. Cushman, S. W. et al. Molecular mechanisms involved in GLUT4 translocation in muscle during insulin and contraction stimulation. *Adv. Exp. Med. Biol.* **441**, 63–71 (1998).
28. Eguez, L. et al. Full intracellular retention of GLUT4 requires AS160 Rab GTPase activating protein. *Cell Metab.* **2**, 263–272 (2005).
29. Capilla, E. et al. Functional characterization of an insulin-responsive glucose transporter (GLUT4) from fish adipose tissue. *Am. J. Physiol. Endocrinol. Metab.* **287**, E348–E357 (2004).
30. Nedachi, T. & Kanzaki, M. Regulation of glucose transporters by insulin and extracellular glucose in C2C12 myotubes. *Am. J. Physiol. Endocrinol. Metab.* **291**, E817–E828 (2006).
31. Maeda, N. et al. Diet-induced insulin resistance in mice lacking adiponectin/ACRP30. *Nat. Med.* **8**, 731 (2002).
32. Zhang, J. H., Chung, T. D. & Oldenburg, K. R. A simple statistical parameter for use in evaluation and validation of high throughput screening assays. *J. Biomol. Screen.* **4**, 67–73 (1999).
33. Blodgett, A. B. et al. A fluorescence method for measurement of glucose transport in kidney cells. *Diabetes Technol. Ther.* **13**, 743–751 (2011).
34. Cao, Y. A. et al. Shifting foci of hematopoiesis during reconstitution from single stem cells. *Proc. Natl. Acad.Sci. USA* **101**, 221–226 (2004).
35. Saltiel, A. R. & Kahn, C. R. Insulin signalling and the regulation of glucose and lipid metabolism. *Nature* **414**, 799–806 (2001).
36. Szablewski, L. Expression of glucose transporters in cancers. *Biochim. Biophys. Acta* **1835**, 164–169 (2013).
37. Ojelabi, O. A., Lloyd, K. P., Simon, A. H., De Zutter, J. K. & Carruthers, A. WZB117 (2-fluoro-6-(m-hydroxybenzoyloxy) phenyl m-hydroxybenzoate) inhibits GLUT1-mediated sugar transport by binding reversibly at the exofacial sugar binding site. *J. Biol. Chem.* **291**, 26762–26772 (2016).
38. Chavez, A. et al. Precise Cas9 targeting enables genomic mutation prevention. *Proc. Natl. Acad. Sci. USA* **115**, 3669 (2018).
39. Shah, L., Laughlin, S. T. & Carrico, I. S. Light-activated Staudinger–Bertozzi ligation within living animals. *J. Am. Chem. Soc.* **138**, 5186–5189 (2016).
40. Sletten, E. M. & Bertozzi, C. R. Bioorthogonal chemistry: fishing for selectivity in a sea of functionality. *Angew. Chem.* **48**, 6974–6998 (2009).
41. Young, C. D. et al. Modulation of glucose transporter 1 (GLUT1) expression levels alters mouse mammary tumor cell growth in vitro and in vivo. *PLoS ONE* **6**, e23205–e23205 (2011).
42. Wellberg, E. A. et al. The glucose transporter GLUT1 is required for ErbB2-induced mammary tumorigenesis. *Breast Cancer Res.* **18**, 131–131 (2016).
43. Hall, M. P. et al. Click beetle luciferase mutant and near infrared naphthyl-luciferins for improved bioluminescence imaging. *Nat. Commun.* **9**, 132 (2018).

Acknowledgements

We thank the Leenaards Foundation, NCCR Chemical Biology and Swiss National Foundation (grant no. CR23I3_157023) for generous financial support. We thank the laboratory of P. Aebischer for the kind gift of C2C12-luc cells. We thank the laboratory of D. Felsher and A. Stahl for the kind gifts of human embryonic kidney 293 TN and 3T13-L1 cells, respectively. We thank J. Frigell for the synthesis of several GAz derivatives (data not shown). We thank A. Konovalova for performing initial in vitro experiments on GAz probes (data not shown) and help with the technical scale-up of some of the reagents. We also thank P. Gonschorek and B. Mangeat for help with analyzing sequences of *Slc2a1* gene in CRISPR/Cas9-mediated GLUT1 knockout and in negative control. We also thank the laboratory of K. Sakamoto for the kind gift of GLUT4 antibodies. We thank EPFL core facilities for histology, mass spectrometry and nuclear magnetic resonance analysis (in particular, P. Mieville and E. Baudat for technical support).

Author contributions

E.G. conceptualized the study. T.M., G.M., P.K., R.S., A.B. and A.Y. carried out the in vitro and in vivo experiments (except the PET study). N.B., P.K. and R.S. synthesized CLP and various GAz reagents. T.M. and A.B. carried out reaction kinetic studies. D.S., A.J., V.M. and G.A. designed and performed PET imaging experiments. E.G., T.M. and G.M. wrote the manuscript. A.Y., P.K., R.S., A.B., N.B. and D.S. edited the manuscript. E.G. acquired the funding.

Competing interests

The authors declare no competing interests.

Additional information

Supplementary information is available for this paper at https://doi.org/10.1038/s41592-019-0421-z.

Reprints and permissions information is available at www.nature.com/reprints.

Correspondence and requests for materials should be addressed to E.G.

Publisher's note: Springer Nature remains neutral with regard to jurisdictional claims in published maps and institutional affiliations.

Methods

Chemical reagents. Procedures for chemical synthesis and characterization of new reagents are summarized in the Supplementary Information. All chemical reagents obtained from commercial suppliers were used without further purification unless noted. All compounds/solvents were obtained from Sigma-Aldrich except D-luciferin, which was acquired from Promega.

Cell cultures. All the cell lines used in this study were stably transfected with the luciferase gene. C2C12-luc cells were transfected with firefly luciferase gene and were kindly provided by the lab of P. Aebischer (EPFL, Lausanne, Switzerland). Cells were cultured in DMEM (Gibco) supplemented with 10% fetal bovine serum (FBS) and 1% penicillin-streptomycin. We initiated myogenic differentiation in the cells reaching confluence by switching to a medium containing 2% horse serum. The cells were assayed 4 d post-confluency. Then, 4T1-luc cells were obtained from PerkinElmer and transfected with RedLuc luciferase construct. After that, 4T1-luc cells were maintained in RPMI media supplemented with 10% FBS and 1% penicillin-streptomycin. HT1080-luc cells were obtained from PerkinElmer and were transfected with Luc2 luciferase gene. The cells were grown in minimal essential medium supplemented with 10% FBS and 1% penicillin-streptomycin. The cells were stably transfected with luciferase gene construct bearing lentivirus (PerkinElmer, CLS960002) and are referred to here as HT1080-luc cells. The 3T3 L1-luc fibroblasts (ATCC) were cultured in DMEM containing 10% fetal calf serum and 1% penicillin-streptomycin. Cells were seeded with the density of 2,000–3,000 cells per cm^2 and split at 60% density to avoid differentiation. To induce pre-adipocyte differentiation, 2 d post-confluent cells were incubated in differentiation medium (DMEM containing 10% FBS, 1% penicillin-streptomycin, 1 µg ml^{-1} insulin, 0.25 µM dexamethasone, 0.5 mM IBMX and 2 µM rosiglitazone) for 2 d before switching to post-differentiation medium (DMEM containing 10% FBS, 1% penicillin-streptomycin and 1 µg ml^{-1} of insulin) for an additional 2 d. Adipocytes were maintained in DMEM supplemented with 10% FBS and 1% penicillin-streptomycin, and assayed between 8 and 12 d after initiation of the differentiation. All cells were maintained at 37 °C in a 5% CO_2 atmosphere. In all washing experiments, PBS sterile solution was used (Thermo Fisher). All cells were maintained at 37 °C in a 5% CO_2 atmosphere.

Imaging and quantification of D-glucose uptake in living cells using the BiGluc probe. Cells were plated in a black 96-well plate (4×10^4 cells per well) with a clear bottom and assayed the next day or on differentiation (C2C12-luc, 3T3-L1-luc). For experiments, the growth medium was removed and 10 µM CLP in Krebs–Ringer-HEPES buffer (KRH; 50 mM HEPES, 137 mM NaCl, 4.7 mM KCl, 1.85 mM $CaCl_2$, 1.3 mM $MgSO_4$, 0.1% BSA, pH 7.4) or KRH alone was added to the buffer in the wells for 1 h. On incubation, the plates were rinsed twice with PBS, and medium was replaced with 100 µl of the GAz4 probe in KRH buffer or 10 µM D-Luciferin in PBS with or without the GAz4 probe, after which we performed signal acquisition. To investigate signal/background noise ratio, cells were treated with various concentrations of GAz4 in PBS ranging from 5 to 500 µM (Supplementary Fig. 2). Immediately after the addition of GAz4, the plates were imaged using an IVIS Spectrum (PerkinElmer) continuously for 30 min. Bioluminescence was quantified using region of interest (ROI) analysis of the individual wells, and the average signal, expressed as the total number of photons emitted per second per cm^2 per steradian ($s^{-1}\,cm^{-2}\,sr^{-1}$), from each of the wells was calculated using the Living Image 3.2 software (PerkinElmer). We calculated total luminescence by integrating the area under corresponding kinetic curves. The results were adjusted to the mean relative luciferin signal in all cases when treatment with a certain compound (e.g., cytochalasin B) affected luciferase expression. All the uptake measurements were done in triplicate.

In vitro competition and inhibition assays. Here, 4T1-luc, HT1080-luc and C2C12-luc cells were grown as described above (see the 'Cell cultures' section for more details). The medium was removed and the culture plates were rinsed twice with PBS. The cells were then incubated at 37 °C with 10 µM CLP in 100 µl of KRH buffer for 1 h. On incubation, we rinsed the plates twice with PBS, and then we added 100 µM GAz4 with or without either D-glucose or L-glucose at 5 mM and 10 mM in KRH buffer. The cells were immediately placed in the IVIS Spectrum System, and the plates were imaged for 30 min continuously, with one image acquired every minute. The appropriate luciferin controls were done in parallel with competition experiments to take into account effects of experimental conditions (addition of D- and L-glucose) on luciferase expression. Briefly, we rinsed 4T1-luc, HT1080-luc and C2C12-luc cells with PBS and then added 10 µM luciferin with or without either D-glucose or L-glucose at 5 mM and 10 mM in KRH buffer.

To examine the effect of cytochalasin B (endofacial inhibitor), WZB-117 and 4,6-EDG (exofacial inhibitor), we incubated HT1080-luc and 4T1-luc cells with 10 µM CLP as described above, and then washed the cells with PBS. The cells were then pre-incubated with 10 µM cytochalasin B for 10 min, 50 µM WZB-117 for 30 min and 50 mM 4,6-EDG for 30 min followed by the addition of 100 µM GAz4 in KRH buffer. The cells were imaged for 30 min continuously with one image acquired every minute (IVIS Spectrum, PerkinElmer). The controls included uptake in the absence of an inhibitor and luciferin. To take into account effects of cytochalasin B on expression levels of luciferase in both cell lines, we repeated the same experiment using luciferin as a control (10 µM in KRH buffer).

Glucose uptake in 4T1-luc cells inhibited with 4,6-EDG was also measured with a commercially available fluorescent probe, GB2-Cy3 (Spark Biopharma). The protocol for inhibition is described above and was followed by the addition of 100 µM GB2-Cy3 in KRH buffer. The cells were incubated with the probe for 30 min and then rinsed with cold PBS (3×). The fluorescence signal was acquired immediately with the imager (IVIS Spectrum, PerkinElmer) with a Cy3 channel.

Measurement of D-glucose uptake in insulin-stimulated differentiated myotubes and adipocytes (C1C12-luc, 3T3-L1-luc). Bioluminescent light production from BiGluc probe was measured in C2C12-luc and 3T3-L1 cells on their complete differentiation and compared to light production in their non-differentiated controls. Before probe incubation, the cells were starved in serum-free growth medium overnight before treatment with insulin. The cells were washed with KRH buffer and incubated with 10 µM CLP with or without 100 nM insulin in KRH buffer for 1 h, followed by rinsing with PBS (2×) and subsequent addition of 100 µM GAz4 in KRH buffer. The bioluminescence signal was acquired immediately every minute for 30 min continuously. The controls included measurement of BiGluc light production by non-stimulated cells. All the results were adjusted to the mean relative signal obtained from cells treated with luciferin control (10 µM) with and without insulin.

Glucose uptake in insulin-stimulated differentiated myotubes was also measured with a commercially available fluorescent probe, 2-NBDG. The protocol for insulin stimulation is described above and was followed by the addition of 300 µM 2-NBDG in KRH buffer. The cells were incubated with the probe for 30 min, followed by rinsing with PBS (2×). The fluorescence signal was acquired immediately on a plate reader (TECAN) with excitation at 475 nm and emission at 550 nm, as suggested by the reagent provider.

Measurement of D-glucose uptake in the PI3K-dependent pathway with BiGluc probe. Differentiated C2C12-luc cells were incubated for 30 min at 37 °C in a humidified 5% CO_2 atmosphere in medium containing 100 nM wortmannin, then washed with PBS and co-stimulated with 100 nM insulin and 10 µM CLP in KRH buffer for 30 min. On incubation, the cells were washed with PBS, followed by the addition of 100 µM GAz4 in KRH. The cells were immediately imaged for 30 min continuously, with one image acquired every minute. The cells incubated with media lacking wortmannin were used as a positive control. As described above, the results were normalized to the mean relative signal from control cells treated with luciferin (10 µM).

2-deoxy-D-[^{3}H] ([^{3}H]-2DG) glucose uptake in an insulin dose-dependent assay. We analyzed the stimulatory activity of insulin in glucose transport by measuring the cell uptake of [^{3}H]-2DG. Differentiated C2C12-luc cells grown in 24-well plates were washed twice with serum-free DMEM and incubated with 0.5 ml of the same medium at 37 °C overnight. The cells were washed three times with KRH buffer and incubated with insulin in different concentrations ranging from 0 to 200 nM for 30 min. Glucose-uptake measurements were initiated by the addition of 55.5 MBql^{-1} of [^{3}H]-2DG and 1 mmoll^{-1} of regular glucose, as the final concentrations. After 20 min, we terminated the experiment by washing the cells three times with cold PBS and lysing cells with RIPA buffer (50 mM Tris-HCl, 150 mM NaCl, 1% Triton X-100, 0.5% Na-deoxycholate, 0.1% SDS). The radioactivity retained by the cell lysates was measured by an LS 6000 Series Liquid Scintil (Beckman Coulter).

CRISPR/Cas9-mediated GLUT1 knockout in 4T1-luc cells. CRISPR/Cas9-mediated GLUT1 knockout in 4T1-luc cells was done according to the manufacturer's instructions (Santa Cruz Biotechnology, Inc.). Briefly, 5×10^4 cells were plated onto 12-well microplates and allowed to grow to 70% confluence. Next, 20 µg of GLUT1 CRISPR/Cas9 KO Plasmid (sc-422998) was added to 4 µl of UltraCruz Transfection Reagent (sc-395739). The complexes were incubated for 20 min and then overlaid onto the cells. The plates were incubated at 37 °C in 5% CO_2 for 72 h. Transfected cells were sorted on the basis of green fluorescent protein (GFP) fluorescence using a FACSDiva cell sorter from Beckton Dickinson to sort one cell per well into 96-well plates (two plates per batch of transfected cells). The cells were cultured in RPMI medium with 10% FBS and 1% penicillin-streptomycin, and, after 14 d, GFP-expressing colonies were determined by inspection under a microscope equipped with ultraviolet light. Expanded-sorted cell populations were phenotypically analyzed to confirm complete allelic knockout. The Control CRISPR/Cas9 Plasmid (sc-418922) contained non-targeted 20-nucleotide scrambled guide RNA (gRNA), not recognizing any DNA sequence and therefore not binding or cleaving genomic DNA, and was designed as a negative control.

PCR amplification and sequencing of *Slc2a1* amplicons. DNA from 4T1-luc cells, the CRISPR/Cas9 clone knockouts and their negative controls was isolated using the NucleoSpin Tissue Kit (Macherey-Nagel) according to the manufacturer's instructions. Primers that amplified 200- to 400-base-pair regions surrounding the sites of interest (C region (exon 3) and AB region (exon 5) of *Slc2a1* gene) were

selected using the program Geneious Prime (Supplementary Note 3). Genomic loci were amplified with Taq polymerase (BioLabs) using 50 ng of genomic DNA as input. PCR products were cloned into the pCR 4-TOPO cloning vector according to the manufacturer's instructions (Invitrogen Corporation). The TA cloning reactions were transformed by heat shock into DH5α competent cells (Invitrogen Corporation). DNA from ten colonies for each clone was extracted using the QIAprep Spin Miniprep Kit (Qiagen) and sequenced at Microsynth with the company's M13F primer. Sequences were analyzed using Geneious Prime (https://www.geneious.com).

shRNA knockdown. pLKO.1-shRNA-GLUT1 no. 1 (Mission TRC shRNA, TRCN0000079328), shRNA-GLUT1 no. 2 (Mission TRC shRNA, TRCN0000311403), shRNA-GLUT1 no. 3 (Mission TRC shRNA, TRCN0000324209), shRNA-GLUT1 no. 4 (Mission TRC shRNA, TRCN0000305719) and shRNA-GLUT1 no. 5 (Mission TRC shRNA, TRCN0000079332) plasmids were obtained from Sigma. For lentivirus production, human embryonic kidney 293 TN cells were transfected with pLKO.1 shRNA-GLUT1 along with standard packaging plasmids by calcium transfection. Hygromycin-resistant 4T1-luc cells were incubated with viral supernatant containing 4 mg ml^{-1} polybrene. Selection of transduced cells was then performed with 5 mg ml^{-1} puromycin. Targeting sequences for all shRNA are provided in Supplementary Note 4.

Western blot analysis. We prepared protein lysates by lysing cells in RIPA buffer containing protease inhibitor cocktail. The protein concentration was determined using the BCA protein assay (Thermo Scientific), and 30 µg of proteins were separated by SDS–PAGE and transferred to a 0.2-mm nitrocellulose membrane. The membranes were blocked by Tris-buffered saline (TBS; 0.2 M Tris base, 1.5 M NaCl), 0.1% Tween-20 and 5% ECL blocking reagent (GE Healthcare) for 1 h, then incubated with the primary antibody, GLUT1 (Abcam, ab15309), GLUT4 (Santa Cruz, sc-53566), Akt (Cell Signaling, no. 9272), P-Akt (Cell Signaling, no. 9271), heavy chain myosin (Abcam, ab124205) or glycogen synthase (Cell Signaling, no. 3893). Then, the membranes were incubated with HRP-conjugated secondary antibody (Abcam) diluted in TBS with 0.1% Tween-20. After the addition of the HRP substrate, the chemiluminescent signal was detected using a Gel and Blot Imaging System (Azure Biosystems). The same membrane was stripped and reused for detection of β-actin (Abcam, ab8229) or α-tubulin (Sigma, no. T6074) as a loading control, following the same protocol as above.

Cytotoxicity and cell viability assay. Cytotoxicity assays were carried out using a one-step fluorometric assay based on the use of AlamarBlue (Invitrogen). Then, 4T1-luc cells were incubated with a broad concentration range of the GAz4 probe (50 nM–50 mM) for 1 and 24 h followed by 3 h of incubation with AlamarBlue in 96-well microplates at 37 °C in a 5% CO_2 atmosphere. On incubation, the fluorescence of the AlamarBlue was read on a plate reader (TECAN) with excitation at 530 nm and emission at 590 nm.

Cell viability was calculated as a percentage of viable cells and normalized to a dimethylformamide-only control. Cells were incubated with either GAz4 (100 µM) or CLP (10 µM) for varying time intervals (24, 48 and 72 h) at 37 °C and 5% CO_2 (bottom graph in every panel in figures). The intensity of chemiluminescence was measured with an enzyme-linked immunosorbent assay kit according to the manufacturer's instructions (Abcam, ab126572). Results are presented as a mean of three independent experiments.

NAD$^+$ assay. NAD$^+$ was extracted from cells and measured with the EnzyChrom NAD/NADH Assay Kit (BioAssay Systems) according to the manufacturer's instructions.

Experimental animals. We purchased FVB-luc$^{+/+}$ (full abbreviation: FVB-Tg(CAG-luc,-GFP)L2G85Chco/J) mice from Jackson Laboratory and Swiss nu/nu mice from Charles River Laboratories. All animal bioluminescent imaging experiments were reviewed and approved through license 2849 from the Swiss Cantonal Veterinary Office Committee for Animal Experimentation according to the Swiss National Institutional Guidelines. PET imaging animal studies were approved by the University of California Los Angeles (UCLA) Animal Research Committee and were carried out according to the guidelines of the Department of Laboratory Medicine at UCLA.

Imaging and quantification of D-glucose uptake in transgenic reporter mice (FVB-luc$^{+/+}$) using the BiGluc probe. Here, 24 h before imaging, three groups of FVB-luc$^{+/+}$ mice ($n=3$) were pretreated with 100 µl of 1.5 mM CLP reagent dissolved in PBS with 0.1% BSA and fasted for 12 h. The next day the first group was given oral gavage of 100 µl of PBS (control group); the second group was gavaged with 100 µl of GAz4 reagent in PBS in a dose of 12 mg kg^{-1}; and the third group received oral gavage of GAz4 reagent in a dose of 12 mg kg^{-1} in PBS mixed with D-glucose at 1.6 g kg^{-1}. The mice were imaged immediately using a charge-coupled device (CCD) camera (IVIS Spectrum, PerkinElmer) with images acquired every minute for 1 h, continuously. The resulting data were analyzed using the Living Image software, taking the area of the entire body as the ROI.

Insulin tolerance test. FVB-luc$^{+/+}$ mice ($n=4$) were i.v.-injected with 100 µl of 1.5 mM CLP reagent dissolved in PBS with 0.1% BSA. 20 h after CLP injection, the mice were fasted for 4 h and then underwent a 15-min imaging session using a CCD camera (IVIS Spectrum, PerkinElmer) to acquire a background signal. The mice were then i.p.-injected with either a solution of GAz4 in a dose of 12 mg kg^{-1} or GAz4 in a dose of 12 mg kg^{-1} mixed with insulin solution at a final concentration of 0.1 U ml^{-1} in PBS. We imaged the mice immediately using a CCD camera by acquiring images every minute for 1 h, continuously. The resulting data were analyzed using the Living Image software, taking the area of the entire body as the ROI.

CLP clearance study. Mice were i.v.-injected with 100 µl of 1.5 mM CLP reagent dissolved in PBS with 0.1% BSA. After the administration of CLP or vehicle (PBS), blood was collected via heart puncture at three different time points (0, 8 and 24 h) into tubes containing heparin. Plasma was separated by centrifugation at 2,000 r.p.m. for 5 min at 4 °C. GAz4 in a final concentration of 1 mM was added to plasma samples, so the residual CLP could react and produce free luciferin. Next, plasma was added to the cells expressing luciferase (4T1-luc) that were used as a bioluminescent reporter to quantify the amount of free luciferin. Bioluminescence was measured for 30 min using IVIS Spectrum (PerkinElmer). The total photon flux from cells was normalized to 1 µM D-luciferin control to account for different cell numbers.

Imaging and quantification of D-glucose uptake in tumor xenograft models using the BiGluc probe. Imaging of 4T1-luc and 4T1-luc-GLUT1$^{-/-}$ xenografts. Here, 4T1-luc and 4T1-luc-GLUT1$^{-/-}$ no. 1 were harvested, washed twice in PBS and resuspended in 100 µl of serum-free RPMI medium before being inoculated subcutaneously into the dorsal side of the Swiss nude mice ($n=5$) at approximately 1 million cells per mouse. Tumors were measured twice a week, and when the tumor volume reached 65 mm^3, the mice were administered 1.5 mM CLP dissolved in 100 µl of PBS containing 0.1% BSA via i.v. injection. After 24 h, the mice received i.v. injections of GAz4 (12 mg kg^{-1} in 100 µl of PBS). The mice were anesthetized with isoflurane, and the bioluminescence was acquired immediately every minute for 1 h using the auto-exposure mode. The following day, the mice were imaged again on injection of luciferin (15 mg ml^{-1}, 100 µl in PBS) and imaged for 30 min to assure equal light production between the group and control for tumor size. On imaging, mice were killed and the corresponding tumors were dissected for further examination by histological analysis (Supplementary Fig. 15).

Imaging of 4T1-luc xenografts treated with WZB-117 inhibitor. The 4T1-luc cells were harvested, washed twice in PBS and resuspended in 100 µl of serum-free RPMI medium before being inoculated subcutaneously into the dorsal side of the Swiss nude mice ($n=4$) at approximately 1 million cells per mouse. Tumors were measured twice a week, and when the tumor volume reached 65 mm^3, the mice were administered 1.5 mM CLP dissolved in 100 µl of PBS containing 0.1% BSA via i.v. injection. Similar to the previous experiment, the first group received i.v. injections of GAz4 (12 mg kg^{-1} in 100 µl PBS) 24 h after CLP injection. The second group was injected i.p. with WZB-117 (10 mg kg^{-1} in PBS/DMSO (1:1, v/v)) 1 h before administration of GAz4. Both groups were imaged for the duration of 1 h using an IVIS Spectrum camera (PerkinElmer). The following day, the mice were imaged again on i.p. injection of luciferin (15 mg ml^{-1}, 100 µl in PBS) and imaged for 30 min. The total phone flux obtained from each mouse imaged with BiGluc probe was normalized to the signal produced on i.p. injection of equimolar amounts of luciferin (100 µM in 100 µl of PBS) to control for tumor size.

In a separate experiment ($n=4$), we performed measurements of light production from mice that received i.p. injection of luciferin (15 mg ml^{-1}, 100 µl in PBS) with and without WZB-117 inhibitor. Similar to the experiment described above, one group of mice was injected i.p. with WZB-117 (10 mg kg^{-1} in PBS/DMSO (1:1, v/v)) 1 h before administration of luciferin. No difference in signal was observed.

PET imaging. In vivo small animal imaging was conducted at the Crump Institute's Preclinical Imaging Technology Center, UCLA. Mice underwent microPET (GENISYS 8 PET/CT, Sofie Biosciences) and microCT (CrumpCAT, Arion Hadjioannou laboratory) imaging with ^{18}F-fluorodeoxyglucose (^{18}F-FDG). Briefly, mice were injected via the lateral tail vein with radiolabeled probe (70 µCi for ^{18}F-FDG) and then underwent 60-min uptake under 2% isoflurane anesthesia, followed by static microPET and microCT imaging. The microPET images were acquired for 600 s with an energy window of 150–650 keV, reconstructed using maximum-likelihood expectation maximization with corrections for photon attenuation, detector normalization and radioisotope decay (scatter correction was not applied) and converted to units of percentage injected dose per gram (%ID g^{-1}). The microCT images were acquired under 'high resolution' continuous mode using a 50 kilovoltage peak, 200 µA X-ray source and were reconstructed using the Feldkamp algorithm with a voxel size of 125 µm. ROI analysis was conducted using AMIDE v.1.0.5 (ref. [44]) on tumors and select normal tissues (liver, muscle, lung, heart, brain and subcutaneous fat). To account for overall PET probe biodistribution variations between animals, tumor uptake was normalized to the liver for ^{18}F-FDG, as previously described[45].

Immunohistochemistry. The tumors were excised and fixed for 16 h in 10% buffered formalin. The tissues were processed and embedded by the Translational Pathology Core Laboratory at UCLA. Slides were stained in accordance with published protocols[46]. Briefly, following deparaffinization, antigen retrieval was performed by the heat-induced antigen retrieval method following the manufacturers' suggestions for each antibody. We quenched endogenous peroxidase activity by incubating the slides in 3% hydrogen peroxide for 10 min. Blocking was completed with 5% goat serum for 1 h at room temperature. Following incubation with the primary GLUT1 antibody (Alpha Diagnostics no. GT11-A) and secondary antibody, avidin-biotin peroxidase complex (Vector Labs) was used. Finally, staining was visualized using the ImmPACT DAB (Vector Labs). Slides were counterstained with dilute hematoxylin. Following IHC staining, slides were digitally scanned onto a ScanScope AT (Aperio Technologies, Inc.) and images were captured.

Statistical analysis. Statistical analysis was carried out in GraphPad Prism v.8.0.2. Quantitative data are presented as mean ± s.d., if not stated otherwise. Differences were compared using the Student's *t*-test. When *P* values were 0.05 or less, the differences were considered statistically significant.

Reporting Summary. Further information on research design is available in the Nature Research Reporting Summary linked to this article.

Data availability

The data that support the findings of this study are available from the corresponding author upon reasonable request.

References

44. Loening, A. M. & Gambhir, S. S. AMIDE: a free software tool for multimodality medical image analysis. *Mol. Imaging* **2**, 131–137 (2003).
45. Venneti, S. et al. Glutamine-based PET imaging facilitates enhanced metabolic evaluation of gliomas in vivo. *Sci. Transl. Med.* **7**, 274ra217 (2015).
46. Momcilovic, M. & Shackelford, D. B. Targeting LKB1 in cancer—exposing and exploiting vulnerabilities. *Br. J. Cancer* **113**, 574–584 (2015).

nature research

Corresponding author(s): Elena A. Goun NMETH-A36210E

Last updated by author(s): Apr 4, 2019

Reporting Summary

Nature Research wishes to improve the reproducibility of the work that we publish. This form provides structure for consistency and transparency in reporting. For further information on Nature Research policies, see Authors & Referees and the Editorial Policy Checklist.

Statistics

For all statistical analyses, confirm that the following items are present in the figure legend, table legend, main text, or Methods section.

n/a	Confirmed	
☐	☒	The exact sample size (*n*) for each experimental group/condition, given as a discrete number and unit of measurement
☐	☒	A statement on whether measurements were taken from distinct samples or whether the same sample was measured repeatedly
☐	☒	The statistical test(s) used AND whether they are one- or two-sided *Only common tests should be described solely by name; describe more complex techniques in the Methods section.*
☒	☐	A description of all covariates tested
☒	☐	A description of any assumptions or corrections, such as tests of normality and adjustment for multiple comparisons
☐	☒	A full description of the statistical parameters including central tendency (e.g. means) or other basic estimates (e.g. regression coefficient) AND variation (e.g. standard deviation) or associated estimates of uncertainty (e.g. confidence intervals)
☐	☒	For null hypothesis testing, the test statistic (e.g. *F*, *t*, *r*) with confidence intervals, effect sizes, degrees of freedom and *P* value noted *Give P values as exact values whenever suitable.*
☒	☐	For Bayesian analysis, information on the choice of priors and Markov chain Monte Carlo settings
☒	☐	For hierarchical and complex designs, identification of the appropriate level for tests and full reporting of outcomes
☒	☐	Estimates of effect sizes (e.g. Cohen's *d*, Pearson's *r*), indicating how they were calculated

Our web collection on statistics for biologists contains articles on many of the points above.

Software and code

Policy information about availability of computer code

Data collection	Living Image 4.1,
Data analysis	ChemDraw 16.0.1.4 (77), Living Image 4.1, Geneious prime 2019.0.4, Microsoft Word 2016, Microsoft Excel 2016, Microsoft Powerpoint 2016, GraphPad Prism 8.0.2, Adobe Illustrator CC 22.1, Osirix 3.8, EVOS FL Auto, Tecan i-Control 1.11, Nanodrop 8000 2.3.2, cSeries software 1.9.8.0403.

For manuscripts utilizing custom algorithms or software that are central to the research but not yet described in published literature, software must be made available to editors/reviewers. We strongly encourage code deposition in a community repository (e.g. GitHub). See the Nature Research guidelines for submitting code & software for further information.

Data

Policy information about availability of data

All manuscripts must include a data availability statement. This statement should provide the following information, where applicable:

- Accession codes, unique identifiers, or web links for publicly available datasets
- A list of figures that have associated raw data
- A description of any restrictions on data availability

The data that support the findings of this study are available from the corresponding author upon request.

Field-specific reporting

Please select the one below that is the best fit for your research. If you are not sure, read the appropriate sections before making your selection.

☒ Life sciences ☐ Behavioural & social sciences ☐ Ecological, evolutionary & environmental sciences

For a reference copy of the document with all sections, see nature.com/documents/nr-reporting-summary-flat.pdf

Life sciences study design

All studies must disclose on these points even when the disclosure is negative.

Sample size	No sample-size calculations were performed. Sample size was determined to be adequate based on the magnitude and consistency of measurable differences between groups.
Data exclusions	Non of the data were excluded.
Replication	All experiments were repeated at least twice.
Randomization	Mice were randomly divided into experimental groups.
Blinding	Blinding was not relevant to the study, because it would not affect the results.

Reporting for specific materials, systems and methods

We require information from authors about some types of materials, experimental systems and methods used in many studies. Here, indicate whether each material, system or method listed is relevant to your study. If you are not sure if a list item applies to your research, read the appropriate section before selecting a response.

Materials & experimental systems

n/a	Involved in the study
☐	☒ Antibodies
☐	☒ Eukaryotic cell lines
☒	☐ Palaeontology
☐	☒ Animals and other organisms
☒	☐ Human research participants
☒	☐ Clinical data

Methods

n/a	Involved in the study
☒	☐ ChIP-seq
☐	☒ Flow cytometry
☒	☐ MRI-based neuroimaging

Antibodies

Antibodies used	Glut1 (abcam, ab15309, polyclonal, dilution 1:400), Beta-Acitn (abcam, ab8229, polyclonal, dilution 1:1000), donkey anti-goat IgG HRP (abcam, ab97110,polyclonal, dilution 1:10000),Goat anti-Rabbit IgG H&L HRP (abcam, ab97051, polyclonal, dilution 1:10000), Glut4 (abcam, ab654, polyclonal, dilution 1:2000), Myosin (abcam, ab124205,polyclonal, dilution 1:900), Glycogen Synthase (abcam, ab40810, monoclonal [EP817Y], dilution 1:10000), a-Tubulin (Sigma, #T6074Akt, dilution 1:4000), Akt (Cell Signaling , #9271, dilution 1:1000) and P-Akt (Cell Signaling, #9272, dilution 1:1000).
Validation	All the antibodies were validated by the manufacturer.

Eukaryotic cell lines

Policy information about cell lines

Cell line source(s)	C2C12-luc (it was a kind gift form Prof. Patrick Aebischer - LEN, EPFL, Lausanne, Switzerland), HT1080-luc2, 4T1-Redluc, HepG2-luc2 (PerkinElmer), 3T3-L1 (it was a kind gift form Prof. Andreas Stahl, Stanford University) and HEK293 TN (it was a kind gift form Prof. Dean Felsher, Stanford University).
Authentication	None of the cell lines were authenticated.
Mycoplasma contamination	Cell lines were tested with the MycoProbe kit(R&D Systems) and results were negative for mycoplasma contamination.
Commonly misidentified lines (See ICLAC register)	No commonly misidentified cell lines were used.

Animals and other organisms

Policy information about studies involving animals; ARRIVE guidelines recommended for reporting animal research

Laboratory animals	Mus musculus (FVB-Tg[CAG-luc,-GFP]L2G85Chco/ J, females, 12 - 25 weeks, Jackson Lab) Mus musculus (Swiss nu/nu, females, 12 - 25 weeks, Charles river labs)
Wild animals	The study did not involve wild animals.
Field-collected samples	The study did not involve samples collected from the field.
Ethics oversight	Swiss Cantonal Veterinary Office Committee for Animal Experimentation, University of California Los Angeles (UCLA, USA) Animal Research Committee.

Note that full information on the approval of the study protocol must also be provided in the manuscript.

Flow Cytometry

Plots

Confirm that:

☐ The axis labels state the marker and fluorochrome used (e.g. CD4-FITC).

☐ The axis scales are clearly visible. Include numbers along axes only for bottom left plot of group (a 'group' is an analysis of identical markers).

☐ All plots are contour plots with outliers or pseudocolor plots.

☐ A numerical value for number of cells or percentage (with statistics) is provided.

Methodology

Sample preparation	300 000 cells were diluted in 500 ul PBS and sorted for GFP positive.
Instrument	FACSAria Fusion
Software	FACSDiva Version 6.1.2
Cell population abundance	We had population of 785 GFP positive cells that were sorted as 1 cell per well in 96-well plate.
Gating strategy	Describing the gating strategy used for all relevant experiments, specifying the preliminary FSC/SSC of the starting cell population, indicating where boundaries between "positive" and "negative" staining cell populations are defined.

☐ Tick this box to confirm that a figure exemplifying the gating strategy is provided in the Supplementary Information.